Breaking bonds in the atomic force microscope: Extracting information

Felix Hanke and Hans Jürgen Kreuzer[a)]
Department of Physics and Atmospheric Science, Dalhousie University Halifax, Nova Scotia, B3H 3J5, Canada

(Received 3 February 2006; accepted 27 February 2006; published 4 April 2006)

A theoretical framework is developed to analyze molecular bond breaking in dynamic force spectroscopy using atomic force microscopy (AFM). An analytic expression of the observed bond breaking probability as a function of force is obtained in terms of the relevant physical parameters. Three different experimental realizations are discussed, in which (i) the force is increased linearly in time, and (ii) the AFM cantilever is moved at constant speed, and (iii) the force is held constant. We find that unique fitting of the bond parameters such as the potential depth and its width is possible only when data from rather different force-loading rates is used. The complications in the analysis of using the constant velocity mode arising from the intermediate polymer spacer are discussed at length. © *2006 American Vacuum Society.* [DOI: 10.1116/1.2188519]

I. INTRODUCTION

The molecular interactions between small molecular aggregates can be manipulated in nanoarchitectures to construct a molecular switch with bond forming and bond breaking providing the on/off states of a switch, respectively. For a molecular bond with a binding energy E extending over a distance d, the force needed is of the order of E/d. Thus, controlled bond breaking can be achieved at temperatures $T \ll E/k_B$ provided the applied force is controlled to better than $k_B T/d$. For a covalent bond we have $E \sim$ eV and $d \sim$ Å so that the force is of the order of nN and must be controlled at the level of pN.

Bond breaking implies the separation of the two molecular fragments along their reaction coordinate. For a diatomic molecule AB the reaction coordinate is the A-B distance and the energy surface is the intra molecular potential as a function of that distance. For a molecular switch such as the bis-terpyridine moiety TP–Ru–TP separating into TP–Ru and TP fragments[1] their separation involves rotations relative to each other and changes in their internal structures so that the reaction coordinate is to be understood as the minimum energy pathway in a multidimensional coordinate space in which the center of mass separation with local adjustments in relative orientation is the dominant one. Excitations in the rotational and internal vibrational degrees of freedom extend the reaction coordinate into a multidimensional valley in the free energy surface. The latter can and has been calculated for many systems by first principles methods of quantum mechanics. For a simple molecular bond the free energy curve along the reaction coordinate has just one minimum of depth E and width d.[2] For more complex bonds that may entail several unfolding steps before breakage further minima at larger separations appear.[3]

Experimentally controlled bond breakage has been achieved with laser tweezers and with the atomic force microscope (AFM). A typical experiment using single-molecule force microscopy is the recent study of the TP–Ru–TP system[1] in which the TP moieties were first linked to a poly(ethylene glycol) spacer which in turn was attached to the AFM cantilever. Similarly, the spacer of a mono-complexed TP–Ru^{3+} was attached to a suitably prepared surface. In the course of the AFM experiment, the noncomplexed moieties on the tip were brought in contact with the mono-complexed units on the surface resulting in the formation of a bonded bis-terpyridine moiety, TP–Ru^{2+}–TP, in which the Ru atom is reduced. Withdrawing the tip first stretched the spacers and eventually led to the breaking of one of the Ru–TP bonds. In a typical experiment the cantilever speed was around 120 nm/s which led to average bond breaking forces of the order of 100 pN and a statistical width of the force distribution of the order of 50 pN. At this pulling speed, the cantilever forces the system away from equilibrium so that the distribution of bond-breaking forces depends strongly on the velocity used.

Several studies have been published that model dynamic force spectroscopy as described in the last paragraph. An initial molecular dynamics study of bond breaking in proteins[4] suggested that it might be possible to model the reaction paths exactly for extremely fast loading rates or pulling speeds. The most widely cited approach to model this type of experiment was put forward by Evans and Ritchie,[5] who used a simplified form of the bond potential in order to calculate the loading-rate dependent breaking probability. Various authors have since extended this model taking into account rebinding,[6] multiple strands,[7] specific force profiles,[8] and to describe experiments with a constant force loading rate.[9,10] A lot of data have been analyzed recently with the help of Monte Carlo simulations.[11]

A problem that has not received enough attention concerns the uniqueness of modeling any data for the purpose of extracting underlying microscopic parameters. This will be done in this paper by setting up an analytic theory, based on previous work,[9] that can explain breaking force distributions and can be used to extract the relevant physical parameters, such as activation energies, attempt frequencies and

[a)]Author to whom correspondence should be addressed; electronic mail: h.j.kreuzer@dal.ca

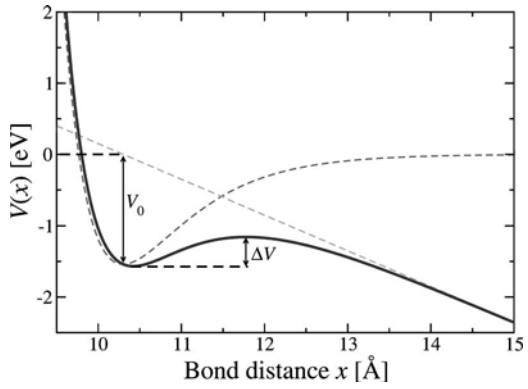

FIG. 1. Bond potential under an external force (blue, solid line) is the linear combination of the unperturbed Morse potential (red, dashed line) and an external force $V_{\text{force}}=-f(x-x_0)$ (green, dashed line). The resulting force-dependent barrier is shown as ΔVs.

bond lengths, from experimental data. We will delineate a set of criteria to ensure uniqueness of such a procedure. Concentrating on bond breaking with the AFM, we examine the different experimental modes including the constant velocity,[1] the constant force-loading rate, or force ramp,[12] setups, and the force-clamp mode.[3]

II. THEORY

We treat bond breaking by an external force as a thermally activated process for which we write down an Arrhenius rate equation for the probability, $P(t)$, that the molecule is still intact at time t[9]

$$\frac{dP}{dt} = -A\,\exp[-\beta\Delta V(f)]P. \tag{1}$$

Here $\Delta V(f)$ is the activation energy or energy difference between the free energy minimum of the bond and the barrier to be overcome in bond breaking under the influence of an applied force, see Fig. 1. The prefactor A contains information about the changes in entropy due to the breakup of the molecule and also about the internal energy redistribution into the bond that eventually breaks. According to transition state theory it is given by $A=\kappa\nu q^*/q$ where ν is the attempt frequency, κ the accommodation coefficient and q^*/q the ratio of the internal partition functions of the activation complex to that of the molecule in the initial state. In the simplest scenario ν can be interpreted as the attempt frequency to break the bond, i.e., roughly that of the oscillations around the minimum of the bond potential, which *in vacuo* is given by

$$\nu = \frac{1}{2\pi}\sqrt{\frac{2V_0\gamma^2}{\mu}}, \tag{2}$$

where μ is the reduced mass of the two fragments and V_0 the maximum depth of the potential. The frequency ν is typically around 10^{12} s^{-1} but it is drastically reduced in a liquid mostly due to solvation effects. In addition, the accommodation coefficient is typically much smaller than unity for a reaction in a liquid and the ratio of the partition functions is significantly smaller than unity so that one expects $A \ll \nu$. What is usually measured in an experiment is not the probability of the bond still being intact at time t but the probability that the bond is broken at time t, $P_b(t)=1-P(t)$.

In the force ramp mode, the force f is increased linearly in time with a force loading rate α

$$f = f_0 + \alpha t. \tag{3}$$

Eliminating t in favor of f we rewrite the Arrhenius rate Eq. (1) as

$$\frac{dP}{df} = -\frac{A}{\alpha}\exp[-\beta\Delta V(f)]P, \tag{4}$$

which can be solved analytically to give

$$P(f) = \exp\left[-\frac{A}{\alpha}\int_{f_0}^{f}\exp[-\beta\Delta V(f')]df'\right] \tag{5}$$

or

$$P(t) = \exp\left[-A\int_0^t \exp[-\beta\Delta V(f_0+\alpha t')]dt'\right]. \tag{6}$$

We obtain the distribution of bond breaking forces by taking the derivative of $P_b(f)=1-P(f)$. Its maximum gives the most probable bond breaking force, and is obtained by equating the second derivative of Eq. (5) to zero, which yields

$$\left.\frac{d\beta\Delta V}{df}\right|_{f_b} = -\frac{A}{\alpha}\exp[-\beta\Delta V(f_b)]. \tag{7}$$

Likewise, we calculate the width of the breaking force distribution by setting the third derivative equal to zero.

To go further analytically we need to specify the bond potential $V(x)$ to obtain $\Delta V(f)$. For a simple bond the Morse potential is known to capture its essential features including the all important dissociative state at large separation (which a harmonic potential obviously does not). In the presence of an external potential it reads

$$V(x) = V_0\{\exp[-2\gamma(x-x_0)] - 2\exp[-\gamma(x-x_0)]\} - f(x-x_0). \tag{8}$$

Here γ^{-1} is the range of the potential, $-V_0$ its depth and x_0 the position of its minimum. From the force-dependent local minimum and maximum of the potential (8) we can calculate the dissociation barrier

$$\Delta V(f) = V_{\max} - V_{\min} = -f(x_+ - x_-) + V_0\{\exp[-2\gamma(x_+ - x_0)] - \exp[-2\gamma(x_- - x_0)] - 2\exp[-\gamma(x_+ - x_0)] + 2\exp[-\gamma(x_- - x_0)]\}. \tag{9}$$

The exponential argument is given by

$$\gamma(x_\pm - x_0) = \ln 2 - \ln\left[1 \mp \sqrt{1-\frac{2f}{\gamma V_0}}\right]. \tag{10}$$

Note that the barrier is not dependent on x_0; $f_{\max}=\gamma V_0/2$ is the maximum force at which the barrier goes to zero, which,

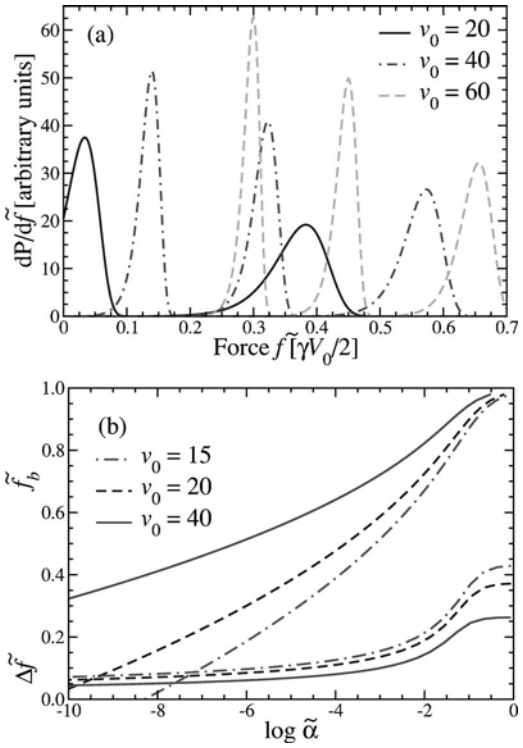

FIG. 2. (a) Breaking force distribution $dP(\tilde{f})/d\tilde{f}$ for three potential depths (as shown by the colors) and for three force loading rates $\tilde{\alpha}=\alpha/(\gamma A V_0)=10^{-10},10^{-5},10^{-1}$ (left to right within each group). Notice that the peak for $\tilde{\alpha}=10^{-10}$ would be so low that all systems essentially dissociate at zero force, see plot (b). (b) Most probable breaking force and width of the force distribution as a function of force load rate for three potential depths (all in dimensionless form).

however, can only be reached by applying the force adiabatically at zero temperature. Explicitly we get for the barrier

$$\Delta V/V_0 = \sqrt{1-\tilde{f}} - \tilde{f}\,\tanh^{-1}\sqrt{1-\tilde{f}}, \tag{11}$$

where $\tilde{f}=f/f_{\max}$. One can show that this function can be approximated to within a few percent over its complete range $0<\tilde{f}<1$ by

$$\Delta V \simeq V_0(1-\tilde{f})^2. \tag{12}$$

It turns out that the approximation (12) is remarkably good for a variety of possible bond potentials, as long as one chooses V_0 to be the depth of the unperturbed potential and defines the dimensionless force in terms of the maximally possible force for a given potential. For example, in the case of a Lennard-Jones potential

$$V(x) = 4\varepsilon\left[\left(\frac{\sigma}{x-x_0}\right)^{12} - \left(\frac{\sigma}{x-x_0}\right)^{6}\right] \tag{13}$$

we would have $V_0=\varepsilon$ and $f_{\max}=(7/26)^{7/6}(144\varepsilon/13\sigma)$. A cutoff harmonic potential as it is used in the Ritchie–Evans model satisfies Eq. (12) exactly, as we show in Appendix A.

The form (12) allows us to do the integral in our force distribution (5) explicitly to find

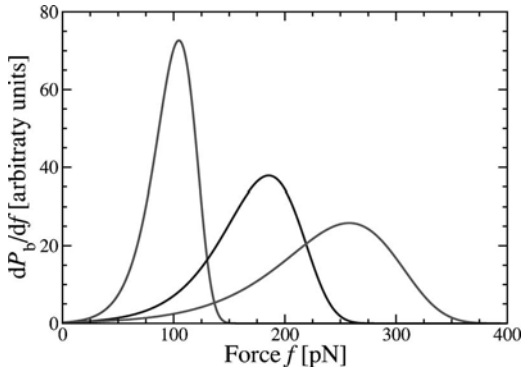

FIG. 3. Theoretical predictions of the breaking force distribution for single, double and triple strands (left to right) for TP–Ru–TP. Same parameters for all curves.

$$P(\tilde{f}) \simeq \exp\left[-\frac{A}{2\alpha}\sqrt{\frac{\pi}{\beta V_0}}f_{\max}\{\mathrm{erf}(\sqrt{\beta V_0}) - \mathrm{erf}(\sqrt{\beta V_0}(1-\tilde{f}))\}\right]. \tag{14}$$

The most probable breaking force f_b is calculated from from the equation

$$1 - 2\frac{f_b}{\gamma V_0} = \frac{\gamma A}{4\beta\alpha}\exp\left[-\beta V_0\left(1-2\frac{f_b}{\gamma V_0}\right)^2\right]. \tag{15}$$

III. RESULTS: FORCE RAMP

The rates $dP_b(f)/df=-dP(f)/df$, or the breaking force distributions, are shown in Fig. 2(a) for three potentials and three values of $\tilde{\alpha}=\alpha/(\gamma A V_0)=1$, 10^{-5}, 10^{-10} and $v_0=V_0/k_BT=20,40,60$. The shapes of these curves are certainly in qualitative agreement with the experimental results, including their slight asymmetry.

To get a quantitative understanding we plot in Fig. 2(b) the most probable breaking force and the width of the force distribution as a function of $\tilde{\alpha}$. From Eq. (15) we see that as $\tilde{\alpha}\to\infty$ the most probable breaking force $\tilde{f}_b$ goes to 1. This occurs either if the loading rate α is very large or if the attempt frequency A is very low. But note that in this case one does not obtain the experimentally observed breaking force distributions.

A fit of our theory to the experimental results of the TP–Ru–TP complex[1] is shown in Fig. 3 with best parameters $\tilde{\alpha}=2\times10^{-5}$ and $v_0=14$. This implies that $V_0=0.35$ eV and $\gamma V_0\simeq 0.5$ eV/Å$=0.7$ nN. From $\tilde{\alpha}$ we obtain $A=6\times10^5$ s^{-1}. Also shown in Fig. 3 are our predictions of multiple bond breaking for the situations where the AFM tip has picked up two and three complexes. Following the experimental paper[1] we assume that by the time the first bond breaks the force is so high that the other bonds break instantaneously. This implies that in Eq. (14) we need to replace f by $f/2$ and $f/3$, respectively, shifting the original peak from 103 pN to 185 and 255 pN. This procedure also widens the peaks asymmetrically, in excellent agreement with experiment.

Next, we would like to make the connection with the Ritchie–Evans version of Bell's model[5,13] employed in numerous experimental papers for the data analysis, for which the rate Eq. (1) reads

$$\frac{dP}{dt} = -k^*_{\text{off}} \exp[\beta f \Delta x_e] P, \tag{16}$$

where Δx_e is interpreted as the maximum elongation of the molecule in quasi-equilibrium before breaking. Note that Δx_e is not a constant (as frequently assumed) but a function of f (as it is in our theory). We obtain this simplified model from the present theory if we assume that the breaking force is much smaller that the maximum, i.e., $f \ll \gamma V_0/2$, which is generally applicable for small loading rates. In this case we can expand the Arrhenius rate Eq. (4) using our harmonic approximation (12) and obtain the rate expression (16) with $\Delta x_e = 4/\gamma$ and

$$k^*_{\text{off}} = A \exp[-\beta V_0]. \tag{17}$$

Recall that the prefactor in Equation (1) has a simple physical meaning: it is an attempt frequency weighted by entropic factors as discussed in Sec. I. On the other hand, k^*_{off} includes a Boltzmann weight involving the potential depth V_0. Thus it is a hybrid that appears to defy physical interpretation if V_0 is not explicitly known.

The expressions for Δx_e and k^*_{off} above enable direct comparison with the TP–Ru–TP data by Kudera *et al.*,[1] where we can use our values for A, V_0 and γ to get $\Delta x_e = 2$ Å, and $k^*_{\text{off}} = 0.5\ \text{s}^{-1}$, agreeing with their values of 3.3 Å and $0.05\ \text{s}^{-1}$ to within an order of magnitude. The reason for these discrepancies in the two parameters k^*_{off} and Δx_e is the approximate nature of the Ritchie–Evans model: the data extend over an interval $f_b \pm \Delta f/2$, and do not satisfy the condition $f \ll \gamma V_0/2$ for the top 20% of this range.

In concluding this discussion we note that the Ritchie–Evans model lacks an important physical parameter, namely the strength of the bond. It thus appears to be limited to forces with $f \ll \gamma V_0/2$, a restriction not imposed in our general model. We will show in Sec. IV below, that it is advisable to use force loading rates as large as technically possible. This would hopefully enable observations close to the maximally possible force $f_{\max}$ and should facilitate the extraction of microscopic parameters.

IV. DATA ANALYSIS: FORCE RAMP

Our theory of bond breaking has three independent parameters A, V_0 and γ in terms of which the probability of finding and intact bond (14) reads

$$P(f) \simeq \exp\left[-\frac{A}{4\alpha} \gamma V_0 \sqrt{\frac{\pi k_B T}{V_0}} \left\{ \text{erf}(\sqrt{V_0/k_B T}) - \text{erf}\left(\sqrt{V_0/k_B T} \left(1 - 2\frac{f_b}{\gamma V_0} \right) \right) \right\} \right]. \tag{18}$$

To extract these parameters from experimental data, one has several options: (i) measure the force distribution for several force loading rates α and fit them with the theoretical curve; and (ii) to measure the breaking force distributions when several strands are attached. A third option, namely to determine the maximum and width of the breaking force distribution for several force loading rates α, is also possible provided data with good statistics are available.

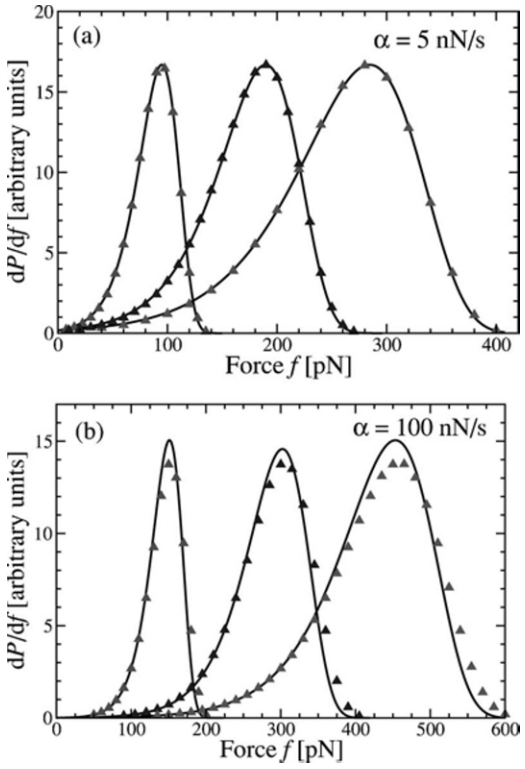

FIG. 4. Numerical fit to generated data ($V_0/k_B = 4200$ K; $A = 10^6\ \text{s}^{-1}$; $\gamma = 1.4\ \text{Å}^{-1}$) that utilized only the input data shown in (a). The same "fit" can be corrected only by taking into account data for a higher force loading rate, as done in panel (b).

We have first checked option (i) and found that a unique fit is obtained if we take three α that span two orders of magnitude. Our experimental *data* were force distributions calculated from Eq. (14). The extracted fit parameters agree with the original input data to arbitrary precision. The uniqueness of the extracted parameters is quickly lost if the force loading rates differ by less than two orders of magnitude. Similarly, option (ii), i.e., measuring the force distributions for several attached strands (for 1, 2, and 3 attached strands) also leads to a unique and perfect fit if two force loading rates are used that differ by one order of magnitude. Notice that we have used input data which were directly derived from Eq. (5), without considering any noise—this is to highlight the difficulty in extracting physically meaningful parameters.

To demonstrate the pitfalls of insufficient data, we have analyzed the force distributions for one, two, and three strands for a single force loading rate α. As Fig. 4(a) shows, we can easily produce a *good* fit; however, the parameters extracted via least-square fitting can be different from the input and strongly depend on the initial guesses in the fitting procedure, i.e., the fit is *not* unique. This is shown in Fig. 4(a) where the input data (triangles) were calculated for

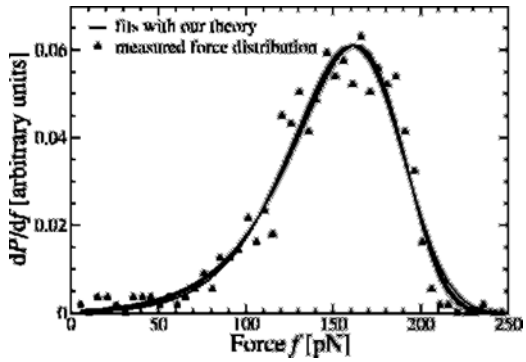

FIG. 5. Unfolding forces for ubiquitin, measured in Ref. 14 and fitted with our theory. All parameters are given in Table I.

TABLE I. Parameters V_0, γ, and A for the ubiquitin experiment, the corresponding k_{off}^* from the Ritchie–Evans model, and the maximum force $f_{\max}=\gamma V_0/2$ for each Morse potential.

V_0 [eV]	γ [Å^{-1}]	A [s^{-1}]	k_{off}^* [s^{-1}]	Δx_e [Å]	$f_{\max}$ [pN]
0.236	1.76	1.06×10^{2}	9.78×10^{-3}	2.27	334
0.273	2.09	8.02×10^{2}	1.75×10^{-2}	1.91	457
0.319	2.29	6.58×10^{3}	2.28×10^{-2}	1.75	585
0.371	2.41	5.78×10^{4}	2.65×10^{-2}	1.66	717
0.403	2.47	2.21×10^{5}	2.82×10^{-2}	1.62	799
0.427	2.51	5.81×10^{5}	2.93×10^{-2}	1.60	857

$V_0/k_B=4200$ K, $A=10^6$ s^{-1}, and $\gamma=1.4$ Å^{-1}. The fit shown yielded, instead, $V_0/k_B=6200$ K, $A=10^9$ s^{-1}, and $\gamma=1.5$ Å^{-1}. However, it is easy to demonstrate that this is wrong by using the same fit parameters for the three curves at a higher α. Figure 4(b) shows that the latter fit is unacceptable.

What we have concluded so far about the analysis of data to extract the underlying physical parameters controlling bond breakage was based on perfect theoretical breaking force distributions. Noise in experimental data and limited statistics complicate the fitting procedure significantly. Thus one can only expect that the data analysis yields a unique set of parameters if lots of data with good statistics are available, in particular spanning a wide range of force loading rates.

A second, even more striking, example is the analysis of unfolding of ubiquitin data, which was recently measured by Schlierf, Li, and Fernandez.[14] The Ritchie–Evans model gives a perfect fit to their data, if the (physically questionable) quantity Δx_e is used as a fitting parameter. We have done the analysis for their data using the model outlined in the previous section. As indicated above, the resulting fit is not unique. In fact, Fig. 5 shows six different numerically equivalent fits. We compare the obtained fit parameters in Table I and calculate the corresponding values of k_{off}^*-and Δx_e in the Ritchie–Evans model as outlined above. The latter are remarkably constant and match those obtained by Schlierf, Li, and Fernandez in the original Ref. 14. The last column in our table shows why the Ritchie–Evans model is such a good approximation for this experiment—all data remain in the limit $f\ll f_{\max}$. Apparently, the information provided by using a single force loading rate is insufficient to determine the actual physical parameters of the system. We point out that a simultaneous analysis, including the same information for a different force-loading rate, should result in unique values of the bond parameters.

The main numerical difficulties with fitting experimental data with the theoretical breaking force distribution arise from the fact that three parameters must be fitted simultaneously. This can be circumvented with an alternative fitting procedure: (a) integrate the experimental breaking force distribution $dP_b(f)/df$ to obtain $P_b(f)$. (b) Plot

$$\ln\left[\frac{1}{1-P_b(f)}\frac{dP_b(f)}{df}\right]=\ln A-\beta\Delta V(f) \tag{19}$$

as a function of f. At the lowest possible force this function approaches $[\ln A-\beta V_0]$ and as the force approaches its maximum it yields $\ln A$. Next fit $[\ln A-\beta V_0(1-f/f_{\max})^2]$ (which should be possible numerically in the small force regime) and get $f_{\max}=\gamma V_0/2$ and thus γ. This way one obtains first estimates for the three parameters which can then be used for the curve fitting described above.

V. DATA ANALYSIS: PULLING AT CONSTANT CANTILEVER SPEED

Pulling at constant cantilever speed is the (experimentally) simpler mode of breaking a molecular bond in that a feedback loop to control the force loading rate is not required. However, it adds considerable difficulties in the interpretation of the data. A detailed knowledge of the elastic response of the polymer spacer itself is required. The rate Eq. (1) now contains an additional integration over all accessible forces

$$\frac{dP_{\mathrm{intact}}(t)}{dt}=P_{\mathrm{intact}}(t)\times\int df' P_f(f',t)A\exp(-\beta\Delta(f')). \tag{20}$$

Here, P_f is the probability of having a force f at time t. As before, the formal solution to this simple differential equation is given by

$$P_{\mathrm{intact}}(t)=\exp\left[\int_0^t dt'\int df' P_f(f',t')A\exp[-\beta\Delta(f')]\right]. \tag{21}$$

For the force ramp mode we simply have $P_f(f,t)=\delta(f-\alpha t)$. In general, the controlled position scenario has finite force fluctuations.[15,16] These become particularly important when the polymer spacer is pulled very fast and equilibrium theories become inapplicable. In such a scenario, one might consider an approach as outlined elsewhere.[17] Restricting ourselves to slow pulling such that the spacer molecule is always in equilibrium, we find[15]

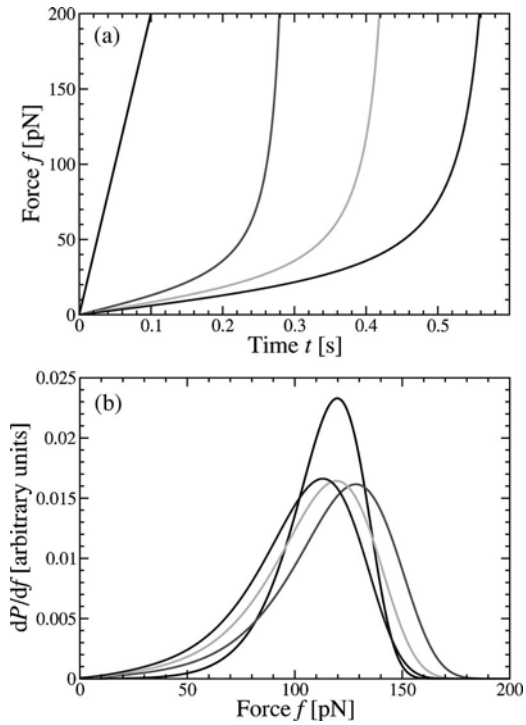

FIG. 6. (a) $f(t)$ traces for a constant force loading rate $\alpha=2$ nN/s (black) compared with constant velocity traces for $v=118$ nm/s with polymer spacers of length $N=100$ (red), 150 (turquoise), and 200 (blue) monomers. These correspond roughly to the spacers used in Ref. 1. (b) The calculated breaking spectra for the same traces as in (a) are done for the parameters $A=4\times10^6$ s^{-1}, $\gamma=1$ Å^{-1}, and $V_0=0.52$ eV.

$$P_f(f,t)=\frac{Z(vt-f/k_c,N,T)\exp(-\beta f^2/(2k_c))}{\int d\bar{f}Z(vt-\bar{f}/k_c,N,T)\exp(-\beta\bar{f}^2/(2k_c))}. \tag{22}$$

Equation (22) requires the canonical partition function of the polymer spacer $Z(L,N,T)$, the pulling velocity v and the cantilever spring constant k_c. Using stiff cantilevers in this case has the advantage that one does not need to care about the fluctuations in the polymer-spacer systems and one can approximate $P_f(f,t)\approx\delta(f-f_{\rm eqm}(vt))$, which we will use in the following analysis. One then needs the force-extension relation, $f_{\rm eqm}(L_p)$, where $L_p=vt$ is the time-dependent length of the polymer spacer. This information is available from experimental data or detailed theories of polymer stretching.[18–20] For a proof of principle, we use the simple freely joined chain model with N monomers of length b whose length L is given in terms of the force f by the Langevin function

$$L(f)=Nb[\coth(\beta fb)-1/(\beta fb)]. \tag{23}$$

Figure 6(a) shows the time dependence of the applied force when the cantilever position is changed at constant force-loading rate and contrasts it with that of a constant velocity experiment. The nonlinearity will affect the breaking force distributions considerably as shown in Fig. 6(b). An additional difficulty arises from the fact that the exact monomer length of the spacer is hard to control and in any given

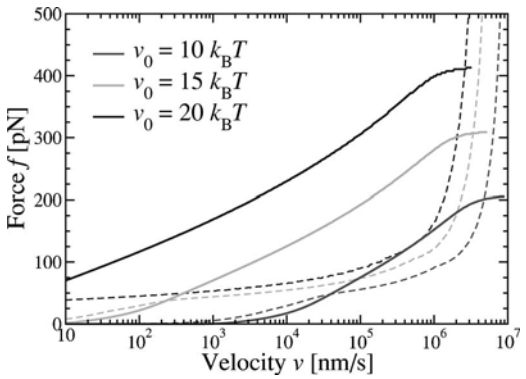

FIG. 7. Most probable breaking force (solid lines) and the width of the dP/df distribution are shown for the case of constant velocities and three different potential depths with $A=4\times10^6$ s^{-1} and $\gamma=1$ Å^{-1}.

experiment will have some distribution over which Eq. (22) must be averaged. We show traces for $N=\{100,150,200\}$ monomers to demonstrate the effect of finite distribution monomer numbers.

There are claims that a Gaussian length distribution leads to no noticeable change in the overall breaking spectra.[11] However, we would like to point out that even a well characterized and narrow length distribution will introduce additional uncertainties in the fitting procedure since it adds two additional parameters, namely the average number of monomers and the distribution width. As pointed out in the last section, one needs very good data for a meaningful interpretation of dynamic force spectroscopy. The finite distribution width of different polymer spacers leads to a slight smearing of the observed distributions, which results in extreme difficulty in the fitting of data. This and other complications related to the use of constant velocity experiments would be completely circumvented by using the force-clamp technique.

VI. FORCE-CLAMP MODE

The force-clamp mode[3] is similar to that with the constant force-loading rate, but here the force is raised rapidly to some value f and held constant. The Arrhenius rate Eq. (1) then has a very simple solution that shows an exponential decay with a constant decay rate

$$P(t)=\exp(-rt),$$

$$r=A\exp[-\beta\Delta V(f)]. \tag{24}$$

In this setup one would have to measure the bond decay time (over several orders of magnitude) many times for each force, which can be used to extract the decay rate r. If we now plot the logarithm of the rate r vs the force f, we find a spectrum such as given in Fig. 8 for four different temperatures. The further analysis then proceeds as discussed around Eq. (19).

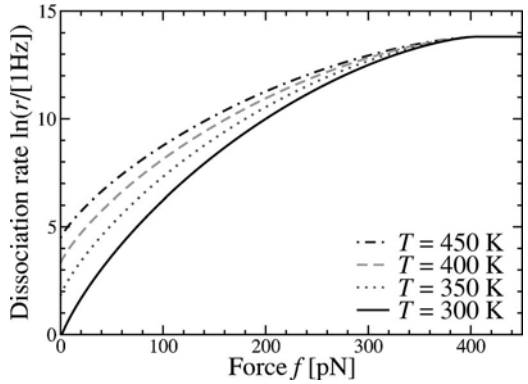

FIG. 8. Force clamp spectra for different temperatures, the parameters are $A=10^6$ s^{-1}, $V_0=0.35$ eV, and $\gamma=1.4$ Å^{-1}. These plots were generated using the barrier $\Delta V(f)$ for a Morse potential as given in Eq. (11).

VII. SUMMARY

We have shown in this paper that a simple analytical theory can be adapted for an analysis of bond breaking in the atomic force microscope. Since the probabilities distribution of bond breaking forces have rather simple shapes and not much structure apart from some asymmetry, a large set of data must be available to obtain the underlying physical parameters such as bond strength, bond width and Arrhenius prefactor uniquely. Extracting the actual shape of the energy surface requires much additional work. A large set of data means data obtained under different experimental conditions such as vastly different force loading rates. Figure 2 shows that increasing the pulling rate will eventually lead to the direct measurement of the maximum bond breaking force. We emphasize that three independent parameters are necessary for a complete microscopic explanation of this situation, compared to two in models derived from Ritchie and Evans' work.

ACKNOWLEDGMENTS

This work was supported by the Office of Naval Research and NSERC. F.H. would like to acknowledge assistance from the Killam Trusts at Dalhousie University.

APPENDIX: CUTOFF HARMONIC BOND POTENTIAL

In this appendix we show that the simplest of bond potentials, namely a cutoff harmonic oscillator, confirms our conclusion that the Evans–Ritchie model is only valid for forces small compared to the maximum forces allowed for a given bond potential.

We assume that the unperturbed bond potential is given by a harmonic potential as $V(x)=-V_0+k(x-x_{\min})^2/2$ so that in the presence of an external force we have

$$V(x) = -V_0 + \frac{1}{2}k(x-x_{\min})^2\theta(\sqrt{2V_0/k}-x) - fx.$$

For purposes of comparison, we choose the force constant to be the same as that for small oscillations in a Morse potential, i.e., $k=2V_0\gamma^2$. Following the procedure outlined in Sec. II we calculate the force-dependent activation energy as

$$\Delta V = V_{\max} - V_{\min} = V_0 - \frac{\sqrt{2V_0}}{k} + \frac{1}{2k}f^2$$

$$= V_0 - \frac{f}{\gamma}\left(1 - \frac{f}{2f_{\max}}\right), \tag{A1}$$

where the maximum sustainable force (for which $\Delta V=0$) is $f_{\max}=2V_0\gamma$. Again we find that $k_{\text{off}}^*=A\exp[-\beta V_0]$. Dropping the quadratic term for forces $f \ll f_{\max}$ we again obtain the Evans–Ritchie model with an activation energy linear in the force and, not surprisingly, no dependence on the depth of the potential. We finally observe that the barrier (A1) in this calculation has the form $\Delta V/V_0=(1-f/f_{\max})^2$, which is exactly the approximation made in Eq. (12).

[1] M. Kudera, C. Eschbaumer, H. E. Gaub, and U. S. Schubert, Adv. Funct. Mater. **13**, 615 (2003).
[2] M. K. Beyer, J. Chem. Phys. **112**, 7307 (2000).
[3] A. F. Oberhauser, P. K. Hansma, M. Carrion-Vasquez, and J. M. Fernandez, Proc. Natl. Acad. Sci. U.S.A. **98**, 468 (2001).
[4] H. Grubmüller, B. Heymann, and P. Tavan, Science **271**, 997 (1997).
[5] E. Evans and K. Ritchie, Biophys. J. **72**, 1541 (1997).
[6] H.-Y. Chen and Y.-P. Chu, Phys. Rev. E **71**, 010901(R) (2005).
[7] P. M. Williams, Anal. Chim. Acta **479**, 107 (2003).
[8] B. Heymann and H. Grubmüller, Phys. Rev. Lett. **84**, 6126 (2000).
[9] H. J. Kreuzer, Chin. J. Phys. (Taipei) **43**, 249 (2005).
[10] M. Evstigneev and P. Reimann, Phys. Rev. E **68**, 045103 (2003).
[11] C. Friedsam, A. K. Wehle, F. Kühner, and H. E. Gaub, J. Phys.: Condens. Matter **15**, S1709 (2003).
[12] P. E. Marszalek, H. Li, A. F. Oberhauser, and J. M. Fernandez, Proc. Natl. Acad. Sci. U.S.A. **99**, 4278 (2002).
[13] G. I. Bell, Science **200**, 618 (1978).
[14] M. Schlierf, H. Li, and J. M. Fernandez, Proc. Natl. Acad. Sci. U.S.A. **101**, 7299 (2004).
[15] H. J. Kreuzer and S. H. Payne, Phys. Rev. E **63**, 021906 (2001).
[16] H. J. Kreuzer, S. H. Payne, and L. Livadaru, Biophys. J. **80**, 2505 (2001).
[17] F. Hanke and H. J. Kreuzer, Phys. Rev. E **72**, 031805 (2005).
[18] F. Oesterhelt, M. Rief, and H. E. Gaub, New J. Phys. **1**, 6.1 (1999).
[19] H. J. Kreuzer and M. Grunze, Europhys. Lett. **55**, 640 (2001).
[20] L. Livadaru and H. J. Kreuzer, Phys. Chem. Chem. Phys. **6**, 3872 (2004).